Using CFD To Understand Chaotic Mixing in Laminar Stirred Tanks

J. M. Zalc, E. S. Szalai, M. M. Alvarez, and F. J. Muzzio
Dept. of Chemical and Biochemical Engineering, Rutgers University, Piscataway, NJ 08855

High-accuracy CFD results for laminar flow in a stirred tank agitated by three Rushton turbines are used as a starting point for an in-depth analysis of mixing. Asymptotic mixing performance is investigated as a function of the Reynolds number by means of Poincaré sections, which reveal large segregated regions with sizes and shapes that vary greatly over a relatively small range of Reynolds numbers. The spatial distribution of mixing intensities is also examined by computing the stretching field, which can be used to optimally choose injection locations for dispersing additives in the tank. When mixing dynamics is examined by particle tracking, the structures observed at short times expose the mechanism of laminar mixing by Rushton turbines. The computed mixing structures are compared with experimental images of dye concentration using planar laser-induced fluorescence. A remarkable agreement is observed for the short-term, as well as the asymptotic evolution, of mixing patterns. Simulations of dye concentration fields as a function of Re confirm large differences in mixing behavior for the four different flow conditions. Strong axial segregation revealed by the stretching field, as well as the location of poorly mixing regions, are accurately predicted.

Introduction

The mixing of liquids in stirred tanks, by either laminar or turbulent flows, is a vital part of many chemical processing operations (Godfrey, 1992). Mixing tends to be a "simple" issue in turbulent flows, where random velocity fluctuations can bring about rapid homogenization. In laminar flows, on the other hand, a globally homogeneous end result is far from guaranteed. Laminar conditions can be unavoidable if the fluids involved are very viscous or shear-sensitive. For instance, laminar flows often occur in bioreactors because of the need to avoid high shear rates that can cause cell damage and diminished process performance (Cherry and Papoutsakis, 1988; Shane et al., 1987), or because of viscosity buildup due to biomass development during the life of the fermentation.

Unfortunately, quantitative methods to describe mixing in stirred tanks have been generally limited to bulk measures such as using neutralization experiments to visually determine mixing time (Hayes et al., 1998; Norwood and Metzner, 1960), or measuring mixing times based on the variance of the pH, conductivity, or concentration recorded by a small number of probes placed in the flow (Kramers et al., 1953; Biggs, 1963). Such methods are intrinsically inaccurate because the probes perturb the flow under study. Electrical resistance tomography has been used to study concentration fields in a stirred tank (Holden et al., 1998), but this method is quite costly and has limited resolution. While laser-induced fluorescence is a promising nonintrusive method for measuring scalar concentration profiles (Distelhoff et al., 1997), this technique needs to be further developed in order to become a fully quantitative method for mixing processes in three-dimensional (3-D) laminar flows. One group (Wittmer, 1998) has developed a method to track the 3-D position of a particle in a stirred vessel for about 1 h. However, a particle large enough to be detected is unlikely to follow the flow closely.

In general, experiments can be costly and time-consuming, especially if a variety of flow conditions and geometric variations are to be considered. With the convenience of increasingly faster digital computers and the efficient implementation of accurate numerical algorithms, computational fluid dynamics (CFD) has emerged as a valuable tool for quickly extracting accurate information about laminar flow and mixing in industrially relevant devices whose complex geometries would have prevented modeling just a few years ago.

Correspondence concerning this article should be addressed to F. J. Muzzio.

Most computational studies of stirred tanks have focused on turbulence modeling (Kresta and Wood, 1991; Sahu et al., 1999; Smith III, 1997; Derksen and Van den Akker, 1999; Naude et al., 1998). Laminar CFD studies in tanks focused largely on the flow field and neglected mixing analysis. For example, Bakker et al. (1996) reported CFD results for laminar flow patterns in a stirred tank with a single pitched blade turbine and attained good agreement with laser doppler velocimetry (LDV) results. Ranade (1997) computed laminar flow fields in a baffled stirred tank with a single Rushton turbine by considering an instantaneous snapshot of the 3-D time-dependent flow. Lamberto et al. (1999) performed an experimental and computational investigation of laminar flow in a single Rushton turbine stirred tank. The computed velocity fields agreed well with particle image velocimetry (PIV) measurements, but a lack of computational speed obviated high-resolution mixing simulations. One group performed sliding mesh simulations of laminar flow in a baffled stirred tank agitated by multiple impellers (Harvey III and Rogers, 1996). The computational results compared well with experimental data, but mixing behavior was not addressed in detail. CFD results for laminar flow in multiple impeller stirred tanks have also been used as the basis for a flow-mapping analysis (Harvey III et al., 2000). However, to the best of our knowledge, no in-depth computational study of laminar mixing mechanisms in a multiple impeller stirred tank has been performed to this date. In particular, controlling the rate and asymptotic efficiency of the mixing processes have not been addressed in detail.

Here, our objective is to explore laminar flow in a multiple-impeller stirred tank, using state-of-the-art CFD tools (Zalc et al., 2002), and to extend the analysis to include short- and long-time mixing performance as a function of the impeller speed. The simulated flow fields are validated extensively by PIV. Planar laser-induced fluorescence (PLIF) is used to compare the experimental and computed mixing patterns. The next section presents the details of the tank geometry and an overview of the computational methods. Results are discussed and conclusions are presented.

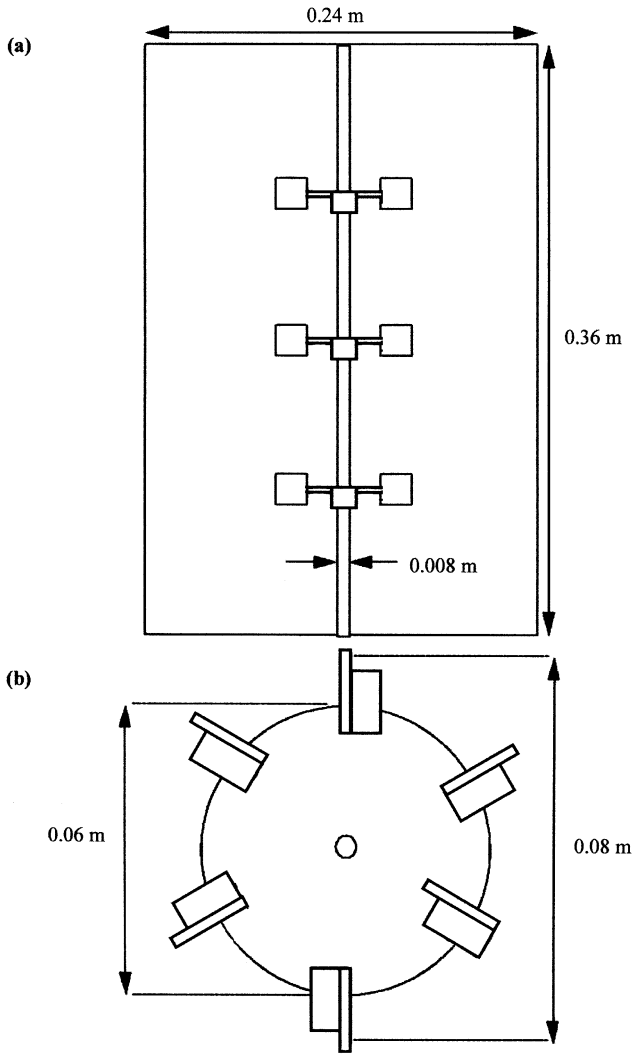

Figure 1. Stirred tank system (a) and (b).

System Geometry and Methods

The system under investigation in the current work is a stirred tank equipped with three six-bladed Rushton turbines (Figures 1a–1b), typical of large-scale fermentations. The tank is a vertical cylindrical vessel with a diameter of 0.24 m and a height-to-diameter ratio of 1.5. Since only laminar flow is considered in this work, an unbaffled tank is chosen as a relevant case study. The shaft has a diameter of 0.008 m and is placed concentrically. The tip-to-tip impeller diameter D_I is 0.08 m. The three impellers are equally spaced in the vertical direction. The working fluid in the experimental system is a glycerine-water mixture with a viscosity μ of 0.4 kg/(m*s) and a density ρ of 1.247 kg/(m^3). The flow condition, represented by the Reynolds number (Re) is given by Eq. 1

$$Re = \frac{\rho N D_I^2}{\mu} \tag{1}$$

The impeller speed N is expressed in RPS. Ten different agitation rates were considered, setting the Reynolds number equal to 20, 40, 60, 80, 100, 120, 140, 160, 180, and 200.

The computations presented in this work were performed using the ORCA CFD package (Dantec Dynamics, Mahwah, NJ). This package includes tools for parametric geometry definition, unstructured tetrahedral meshing, flow field solution, and Eulerian and Lagrangian post-processing routines for mixing analysis. This solver technology has proven to be exceptionally stable for complex flows with second-order accuracy in both the velocity and pressure terms (Zalc et al., 2002a,b). The computational mesh for our system geometry contained 370,340 nodes forming 1,944,799 first-order tetrahedral elements. The residuals for both velocity and pressure during the solution process were required to converge below 10^{-4}. Additional details of the solver technology and post-processing routines, as well as detailed information about accuracy and convergence of the cases presented in this article, are provided elsewhere.

Results

Four types of complementary simulations are used here to examine mixing in the chosen case study. These methods complement one another and make it possible to understand both the short-time dynamics and the asymptotic performance of the mixing process. Poincaré sections, which provide long-time asymptotic information about the size and location of chaotic and nonchaotic regions of the flow, indicate the best mixing performance that the system can achieve as time diverges (neglecting diffusion). However, in general, the practical intent is to mix over short-time scales, for which Poincaré sections are misleading, because they do not provide information concerning the rate or the local efficiency of the mixing process. Nonchaotic regions are typically surrounded by slow mixing layers, and, for short times, they cause much larger heterogeneity than one would surmise from Poincaré sections. Short-time phenomena are examined by doing direct simulations of tracer motion. Different methods are introduced to determine the local microstructure of mixing patterns, and the evolution of the concentration field. Finally, it is shown that much of the observed structure of the mixing process can be understood by analyzing the stretching field generated by the flow. While all four methods follow particle trajectories along the flow, each one requires a different number of particles and a different length of calculation to provide optimal results. Guidance about the selection of practical values for these simulation parameters is provided below.

Poincaré sections

Our primary objective is to quantify differences in convective mixing behavior at different agitation rates, so we first examine asymptotic mixing behavior in the tank by computing Poincaré sections. This analysis identifies regions in the flow that are permanently isolated from the bulk, where mixing occurs only by slow diffusive mechanisms. These segregated regions, commonly referred to as "islands" or "doughnuts," create significant barriers to efficient mixing and their existence is generally undesirable in industrial mixing operations. In order to compute a Poincaré section in a stirred tank, massless fluid tracer particles are distributed in a vertical plane aligned with one of the impeller blades, covering half of the tank cross-section. Particle trajectories are computed by an adaptive stepsize, fourth-order Runge-Kutta integration method, and particle positions are recorded every time a particle crosses a 2-D intersection plane rotating with the impeller. All of the intersections are plotted on one graph. Chaotic regions appear as random-like clouds of points, while regular (nonchaotic) regions look like sets of closed rings or as areas completely devoid of points.

Validation of computational methods is immediately accomplished by comparing the computed Poincaré sections with experimental PLIF measurements (Figure 2). This technique involves injecting a small amount of fluorescent dye in the tank, and illuminating a particular cross-sectional view with a laser. Then, a digital camera is used to take pictures of the evolving mixing pattern, showing how tracer fluid is distributed in the vessel. Half of the vessel cross-section from the center to the tank wall is shown in each picture in Figure 2, where the shaft and the three impeller blades appear on the lefthand side. Figure 2 reveals asymptotic mixing patterns at $Re = 20$ and at $Re = 40$. In each case, the motion of approximately 700 tracer particles were followed for 600 impeller revolutions, which represent a total mixing time of 10 min for $Re = 20$ in (a) and 5 min for $Re = 40$ in (b), respectively. This choice in number of particles and trajectory length represents the best compromise between the need to resolve structural details using a finite amount of computational resources. Excellent agreement is accomplished between the experimental and simulated mixing patterns at both impeller speeds.

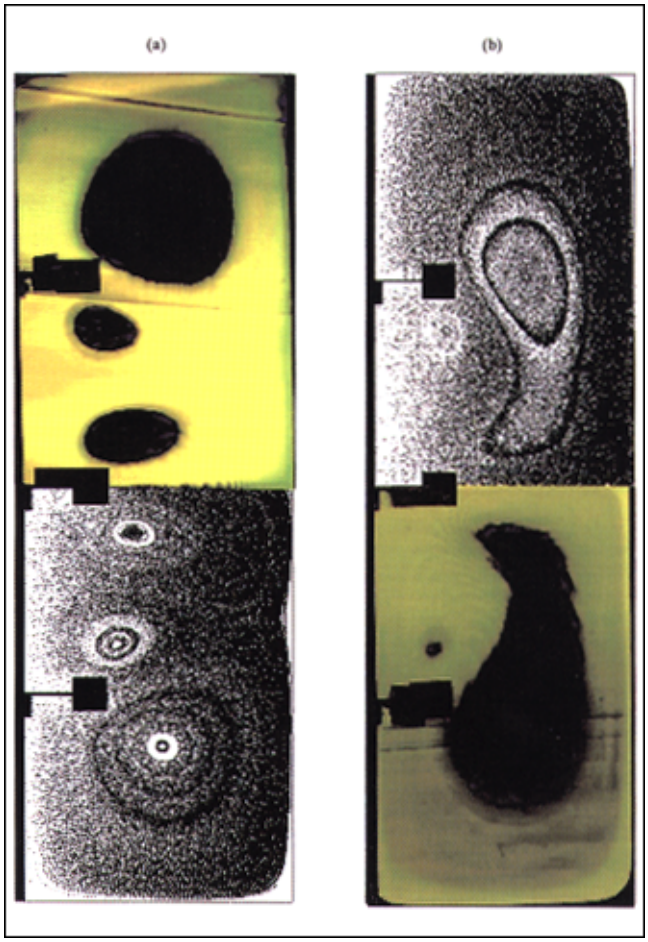

Figure 2. Experimental and simulated mixing patterns after 600 impeller revolutions are compared for $Re = 20$ and 40 in a and b, respectively.

A few features of the experimental and computed Poincaré sections are discussed here in order to provide an illustrative example of flow rate effects on the long-term mixing structures; for full details see Zalc et al. (2002). Poincaré sections have an important role in the assessment of asymptotic mixing performance. Regions that are permanently segregated from the rest of the process fluid are revealed as a concentric ring of particles or empty areas in the flow in the computed mixing patterns. These poor-mixing regions appear as dark spots on the experimental photographs; no dye was initially injected within and no dye can enter except by slow diffusion. It is immediately apparent that the size and position of the

unmixed regions in the computed mixing patterns closely corresponds to those in the experimental photographs. As seen in Figure 2a, six islands of regular flow exist in the tank at $Re = 20$, one above and below the outer tip of each impeller blade. As the impeller speed is increased to 120 RPM ($Re = 40$), two large kidney-shaped islands form in the vessel that extend radially from the impeller assembly. In addition, two small islands are seen, one just below the top impeller blade and the other just above the bottom impeller blade. Laminar flow is often encountered in mixing applications when high-viscosity materials are processed, which means that the diffusivity is generally very low. It is apparent from these figures that homogenization is not accomplished by convective mixing at these flow conditions, and these large segregated regions are practically intact for very long times. Even at the two highest Reynolds numbers examined (at $Re = 80$ and 160), large coherent structures exist in the tank (pictures not shown). Areas where the flow is chaotic, on the other hand, appear as a homogeneous light-colored zone without structure in a Poincaré section, because dye is rapidly distributed everywhere in these regions.

These results indicate that large differences in asymptotic mixing behavior can be encountered at slightly different flow conditions in the laminar regime (a phenomenon known as intermittence). A general rule for *a priori* predictions about mixing performance cannot be established based on the flow field alone. Even if the fluid motion is relatively complex, as in the case of a three-impeller vessel, overall homogeneity is far from assured at constant impeller speed. As discussed in previous publications, the effect of these islands can be great. From a process and equipment design standpoint, a primary interest is to quantify mixing rates at shorter time scales, which are relevant in determining local rates of reaction, material and energy transport, optimal injection points, and so on. Next, the temporal evolution of mixing structures is simulated in order to examine the mechanism of mixing in 3-D periodic chaotic flows.

Mixing structures

The mechanism of stretching and reorientation in stirred tanks is illustrated next by examining the temporal evolution of mixing structures in the tank with Rushton turbines. (To better understand the mixing action of the impellers, consider a tank agitated only with a set of concentric disks on a shaft. It is not surprising that no laminar mixing is possible if only concentric disks are installed (that is, no impeller blades), because such a flow is steady and 2-D, thus incapable of pro-

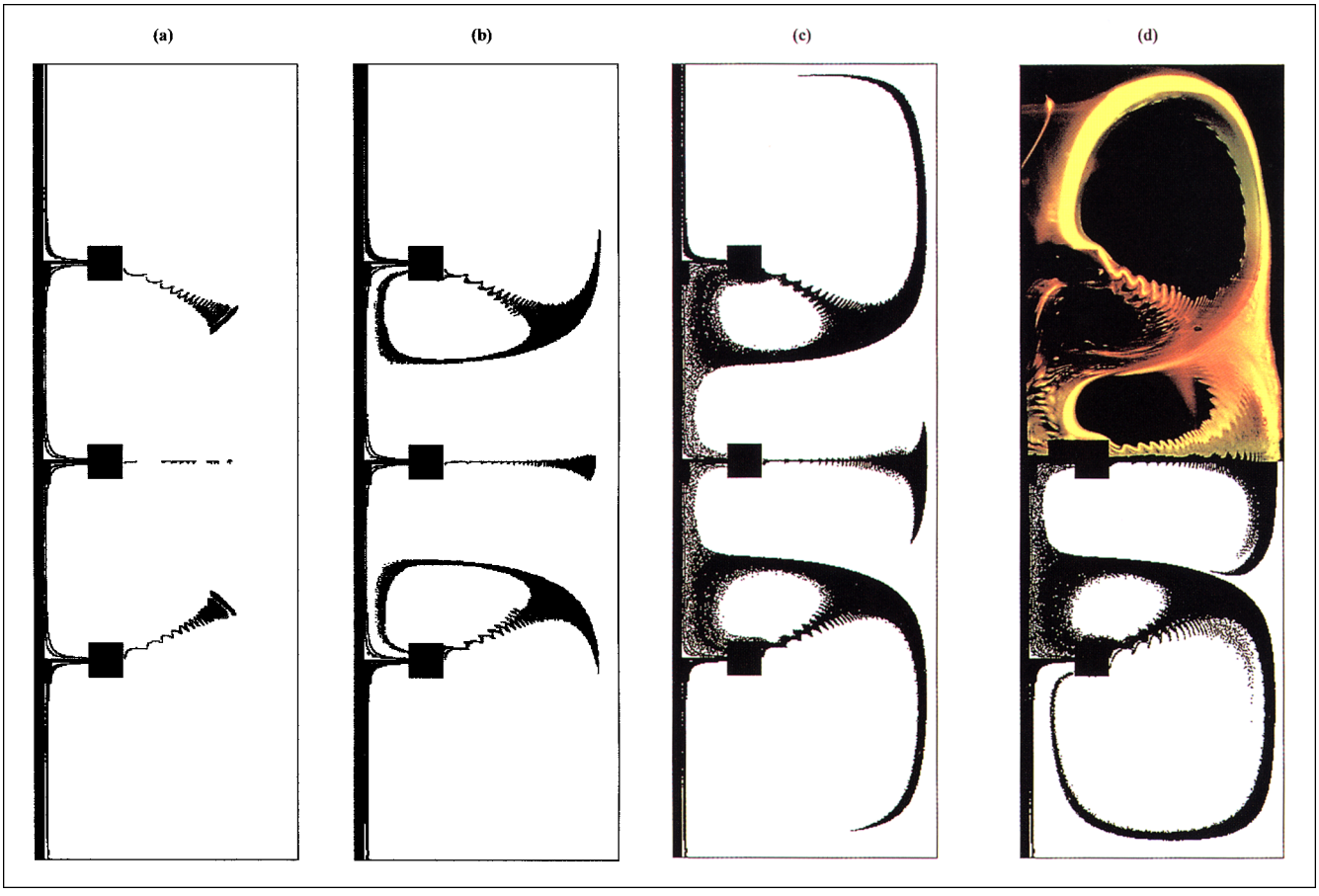

Figure 3. Temporal evolution of partially mixed structures at $Re = 20$.

Results in (a)–(c) represent 10, 20, and 40 impeller revolutions, respectively. In (d), the computational mixing pattern after 60 impeller revolutions (bottom half of figure) is compared with a flow visualization experiment obtained by Planar Laser-Induced Fluorescence (top half of figure).

ducing chaos. These flows are bound to be inefficient for mixing since particle trajectories simply trace out nested tori. There is no exchange of material among the layers by convective mixing.) Simulations were performed by initially placing 30,000 particles along the shaft in a vertical line that extends along the entire height of the tank. All the locations visited by particles are plotted on a single figure. This method provides excellent resolution of mixture structure details while using only a reasonable amount of computer time. Figure 3a shows the mixing structure after 10 impeller revolutions for the flow corresponding to $Re = 20$. Chaotic mixing behavior is created by small periodic perturbations as the passing impeller blades (Alvarez et al., 2002) fold material lines repeatedly. Even after a relatively short time, many particles have passed through the blade region of each impeller and pronounced "wiggle" structures emanate from the top and bottom impellers. All the mixing action of the impellers is due to these small folds created in the near-blade regions. Fluid filaments are folded rapidly by the passing impeller blades, and pushed radially toward the tank wall at successive periods, creating small perturbations in the otherwise steady particle trajectories. (Note that the frequency and amplitude of the wiggles increases with greater distance from the impeller blades.)

These structures appear rapidly, because the tracer particles were initially located along the shaft; for other initial conditions (that is, if they were originally injected near the blade tips), it would take many more impeller revolutions for tracer particles to pass through the impeller regions.

This general observation has an important implication for process design, where additives are distributed in the bulk fluid by injection at a discrete location. It is most beneficial to select an injection location that is upstream of the impellers, so that it will allow the injected material to pass through the impeller blades as early as possible. This is often overlooked in actual chemical processes where material is usually injected at the impeller discharge or near the top surface. While this approach is probably sound for most turbulent systems, it is likely to be inefficient for laminar mixing processes.

Intersections for 20 impeller revolutions are shown in Figure 3b. Here, the mixing structures extend further toward the tank wall than in Figure 3a. By this time, the wiggles created at the top and bottom impellers have wrapped themselves around the smaller toroidal-shaped segregated regions (shown earlier in Figure 2a), creating a classic "horseshoe" structure that is characteristic of chaotic mixing processes. Even though fluid has circulated through each blade region more than once, the top and bottom portions of the vessel are completely devoid of tracer particles, indicating very slow mixing in these regions.

The reorientation and stretching of fluid filaments, further illustrated in Figures 3c–3d after 40 and 60 revolutions, continues as material gradually invades the top and bottom sections of the vessel. The circulation patterns reveal that material is not distributed efficiently in the vertical direction, creating strong axial segregation in the tank. Striking details of the mixing structure after 60 impeller revolutions are seen in the upper half of Figure 3d. The fluorescent tracer material in the experimental PLIF image is bright yellow, and the folds created by the impeller blades show a drastic contrast with the dark regions devoid of dye. The lower half of Figure 3d

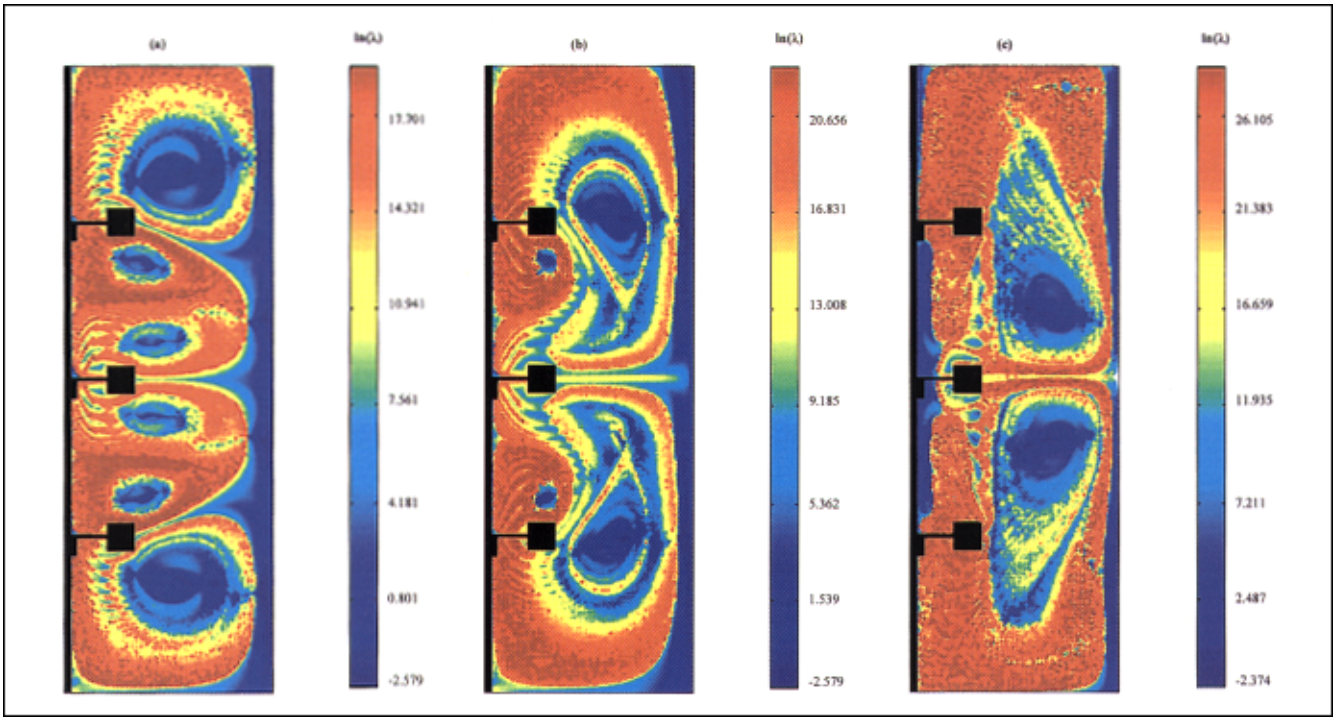

Figure 4. Contour plots of ln(λ) vs. initial position for an initial lattice of 60,000 points showing nonuniformities in mixing intensities in a vertical cross-section of the tank.

Only the right half of the plane is shown after 20 impeller revolutions for $Re = 20$, 40, and 160 in (a)–(c), respectively.

displays the simulated particle positions after 60 impeller revolutions. The comparison between the experimental and numerical short-time mixing structures is excellent. Any minor deviations are attributed to differences in the initial tracer location between experiments and simulations. Such a remarkable level of agreement in the development of partially mixed structures is caused by the Asymptotic Directionality property of chaotic flows. As time increases, every material filament within partially mixed structures of chaotic systems aligns itself exponentially fast with the global hyperbolic manifold of the flow (Muzzio et al., 2000), whose structure is independent of time and initial condition, thus resulting in mixing structures that are independent of initial conditions and that evolve along self-similar templates.

Stretching results

A quantitative measure of mixing intensities in chaotic flows is attained by computing the accumulated stretching of small fluid filaments. These simulations are performed by placing small vectors in the flow. Each infinitesimal vector is deformed by the instantaneous velocity gradient along its trajectory while being convected throughout the flow domain. The elongation experienced by each vector measures the local generation of interfacial area available for transport, and is directly related to the local intensity of mixing. All small vectors placed in regions of chaotic motion yield exponential rates of stretching over time, while ones in regions of regular flow yield stretching rates that are at best linear over time. Further details on the computation of the stretching value λ and the necessary mathematical relationships relating λ to essential mixing parameters are given by Muzzio et al. (1991).

Particle trajectories and accumulated stretching values were computed for an initial lattice of 60,000 passive tracers placed in a vertical cross-sectional plane from the shaft to the outer wall of the tank and spanning the height of the vessel. A small vector, oriented along the vertical direction, is attached to each passive tracer particle. Simulations were run for 360 impeller revolutions and data were recorded at the end of every 20 impeller revolutions. The larger number of particles is needed in order to capture the extremely wide distribution of stretching values with sufficent statistical accuracy. Spatial variations in λ are indicated in Figures 4a–4c, where contour plots of $\ln\lambda$ as a function of initial position are shown after 20 impeller revolutions for each *Re* number in increasing order. In order to generate each contour plot, the tracers were sorted in order of the increasing value of $\ln(\lambda)$. Fluid elements with the lowest values of stretching are plotted in dark blue, followed by light blue, green, yellow, orange and red, which corresponds to points with the highest values of $\ln(\lambda)$. Color ranges are chosen so that each of the 64 colors used in the pictures represents approximately the same number of points. For each case, a logarithmic scale was used for color coding the values according to increasing magnitude, because the stretching increases at an exponential rate in chaotic flows.

Figure 4a illustrates the stretching field for the $Re = 20$ flow, where values of $\ln(\lambda)$ range from -2.579 to 17.701 after just 20 impeller revolutions. Low values of λ exist near the tank wall and in the six islands of regular flow indicated in Figure 2a. Regions of high stretching surround all six of the segregated regions. The largest accumulated stretching is experienced near the blade region of each impeller, where the periodic perturbations generated by the blades were observed. A remarkable feature of the lambda field is its strong symmetry with respect to the plane intersecting the middle impeller. Such planes of symmetry usually reveal flow separatrices that hinder transport. As the *Re* number is increased, higher average values of stretching are observed in the flow, depicted by Figure 4b for the $Re = 40$ case. Here, similar to the lower *Re* case, regions with the lowest stretching match up with poor mixing regions shown in Figure 2b. Figure 4c shows similar contour plots for the $Re = 160$ flow, which has some interesting additional features. A large island surrounding the shaft appears between the top and bottom impellers, which is also observed for $Re = 80$ (not shown). Significant spatial heterogeneity exists in stretching values for all flow conditions. High stretching lines within the low stretching regions and low stretching lines within the high stretching regions are observed. The former (high stretching lines within the low stretching regions) represent narrow layers of chaos within large, multilevel nonchaotic regions. The latter (low stretching lines within the high stretching regions) are caused by compact branches of the stable manifold pervading the chaotic region. Of particular interest among these is the separatrix between the upper and lower regions, caused by a surviving unperturbed manifold structure connecting the parabolic line at the impeller midplane and that at the tank wall. This structure survives due to the existence of a plane of symmetry with respect to the central impeller. Similarly to $Re = 20$, the cases for $Re = 40$, 80 and 160 all display a correspondingly symmetric flow. From the overall structure of the stretching field, we anticipate a strong segregation of tracers in the vertical direction. This topological feature, which is revealed in all its beauty by the stretching field, has grave consequences, as seen below.

The values in Figures 4a–4c span several orders of magnitude. This nonuniform distribution of local mixing intensities is a permanent feature of chaotic mixing flows that results in significant variations in the local rate of reaction and selectivity in reactive industrial processes. Knowing the spatial distribution of stretching can be used to select an efficient injection location for an additive or reactant in a process. Examining the field of mixing intensities in Figures 4a–4c suggests that distributing additives rapidly and efficiently can be accomplished by injecting material along the shaft. As shown in Figure 3, this hypothesis is confirmed by both experiments and simulations of tracer mixing.

It is instructive to look at the distribution of mixing intensities in a quantitative manner by computing the probability density function (PDF) of the logarithm of the stretching values $H_n(\ln(\lambda))$

$$H_n(\ln\lambda) = \left(\frac{1}{N_p}\right)\frac{dN(\ln\lambda)}{d\ln\lambda} \tag{2}$$

where $dN(\ln(\lambda))$ is the number of vectors that have stretching values between $\ln(\lambda)$ and $\ln(\lambda) + d(\lambda)$, and N_p is the total number of stretch vectors. In physical terms, $H_n(\ln(\lambda))$ represents the spectrum of intensities in the micromixing process.

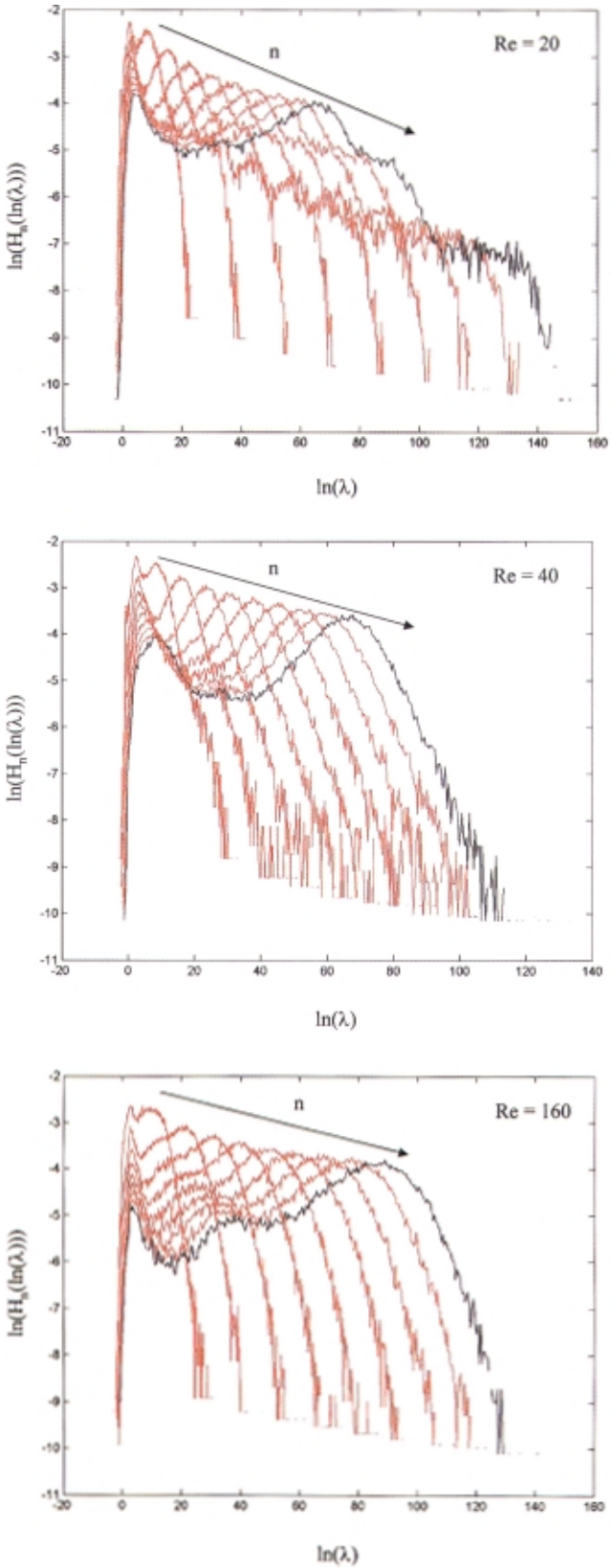

Figure 5. Probability density functions of cumulative stretching values for $n = 40$, 80, 120, 160, 200, 240, 280, 320, and 360 impeller revolutions.

Figures correspond to $Re = 20$ (a), 40 (b), and 160 (c).

Figure 5a shows plots of $\ln(H_n(\ln(\lambda)))$ vs. $\ln(\lambda)$ for the $Re = 20$ flow after 40, 80, 120, 160, 200, 240, 280, 320, and 360 impeller revolutions. The distribution curves shift toward higher stretching values as the total number of revolutions increases. The black curve represents the distribution function after 360 impeller revolutions. As stretching accumulates, the curves broaden, but retain a constant shape.

Figures 5b and 5c show similar results for $Re = 40$ and 160, respectively. In all cases, the distributions exhibit multiple peaks (with mean values in the low and high stretching regions). The distinct peaks near $\ln(\lambda) \sim 0$ for each Re number represent the stretching experienced by filaments initially placed within the segregated regions in the flow. These peaks of low stretching values remain virtually fixed as n increases, because the stretching inside the islands increases at a slow linear rate, if at all. These results are qualitatively identical to those observed in a variety of 2-D flows, suggesting that 3-D chaotic mixing processes in tanks possess much of the same characteristics as 2-D time-dependent chaotic flows.

The average rate of stretching in chaotic flows provides a quantitative basis of comparison for overall mixing efficiency. The arithmetic average $\bar{\lambda}$ and the geometric average $\langle \lambda \rangle$ of the accumulated stretching values after a particular number of impeller revolutions are computed as

$$\bar{\lambda} = \sum_{i=1}^{N_p} \lambda_i / N_p \quad \text{and} \quad \langle \lambda \rangle = \left(\prod_{i=1}^{N_p} \lambda_i \right)^{1/N_p} \tag{3}$$

$N_p = 60{,}000$ stretching vectors are used in this calculation. If the chaotic region of a flow domain is finite, then both $\bar{\lambda}$ and $\langle \lambda \rangle$ grow exponentially (after a brief transient), which is a distinct identifying feature of chaotic dynamics. The average growth rates for $\bar{\lambda}$ and $\langle \lambda \rangle$ are expressed as

$$\bar{\lambda} \approx \alpha^* e^{\Theta n} \quad \text{and} \quad \langle \lambda \rangle \approx \beta^* e^{\Lambda n} \tag{4}$$

Here, the coefficients Θ and Λ, which represent the growth rates for the logarithm of the arithmetic mean and the geometric mean of λ, are known as the topological entropy and Lyapunov exponent, respectively. For details on their meaning and use, see Alvarez et al. (1998) and Muzzio et al. (2000).

Both the arithmetic average $\bar{\lambda}$ and the geometric average $\langle \lambda \rangle$ are needed because they capture different aspects of the physics of mixing. From a statistical point of view, the geometric mean provides a much better behaved and more representative characterization of the stretching rate of individual tracers, that is, it captures the most probable rate of elongation measured when the chaotic region is homogeneously sampled. On the other hand, an essential issue is to determine the growth of the interface between two fluids. This rate is captured by the arithmetic average, $\bar{\lambda}$, which measures the growth of a macroscopic interface as it is convected by the flow. The reason for the difference is that, as the mixing process advances, the interface is distributed nonuniformly by the flow, and its sampling is no longer captured by homogeneously distributed tracers. In other words, while Λ represents the asymptotic rate of stretching of individual particles

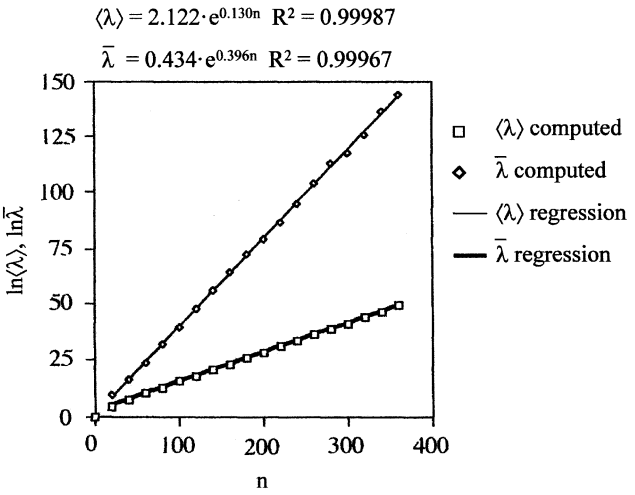

Figure 6. Geometric and arithmetic mean of stretching as a function of the number of impeller revolutions for *Re* = 20.

The slopes of the curves represent the Lyapunov exponent (λ) and the topological entropy (Θ) of the flow, respectively.

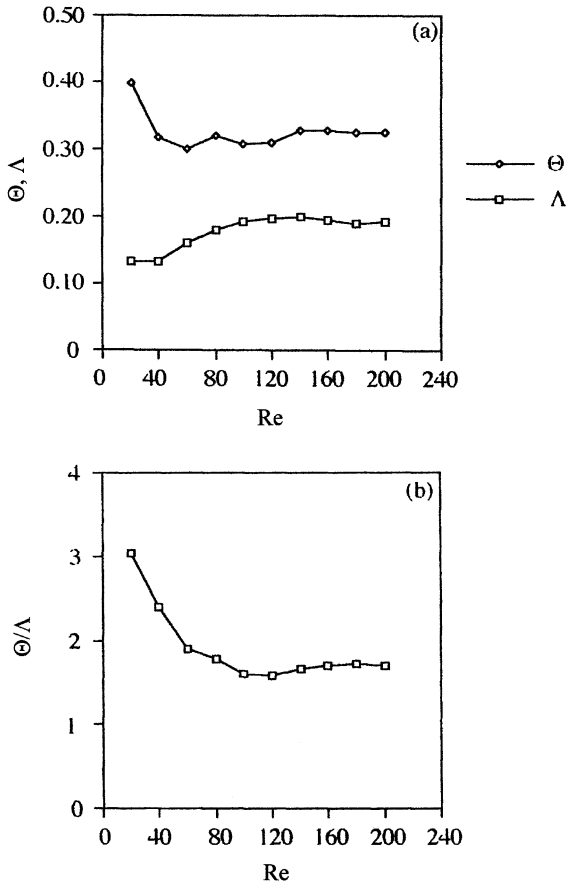

Figure 7. (a) Overall mixing efficiencies-in terms of Λ and Θ as a function of Reynolds number; (b) Ratio of Θ to Λ, plateau in the overall mixing rate at higher Reynolds numbers.

homogeneously distributed throughout the chaotic region, the topological entropy quantifies the short-time rate of intermaterial area growth and thus represents the true rate of mixing in the system (Alvarez et al., 1998; Muzzio et al., 2000). The fact that $\bar{\lambda}$ is poorly behaved numerically, requiring extensive calculations for its accurate determination, is unfortunate, but its use is unavoidable.

Figure 6 illustrates the growth of $\ln\bar{\lambda}$ and $\ln\langle\lambda\rangle$ as a function of the number of impeller revolutions for the $Re = 20$ case. A least-squares linear regression is performed to determine the slopes, yielding the coefficients Θ and Λ. In Figure 6, both the logarithm of the arithmetic mean ($\ln\bar{\lambda}$) and the geometric mean ($\ln\langle\lambda\rangle$) increase linearly with correlation coefficients greater than 0.999. A faster rate of increase is observed for $\ln\bar{\lambda}$ than for $\ln\langle\lambda\rangle$ (that is, $\Theta > \Lambda$ for all *Re* numbers), which is consistent with previous findings for 2-D chaotic periodic flows (Alvarez et al., 1998).

Λ and Θ are computed for each impeller speed to determine the effects of Reynolds number on mixing efficiency, and the results are summarized in Figure 7a. The average rates approach a plateau near $Re = 100$, indicating that increasing the agitator speed beyond this point does not contribute to increased mixing performance in the laminar regime. In Figure 7b, the ratio (Θ/Λ) is shown as a function of the Reynolds number. Θ/Λ is highest for $Re = 20$ and drops sharply with increasing *Re* number until $Re = 100$, beyond which the ratio is fairly constant.

Blob dispersion simulations

Stretching fields reveal valuable information about mixing processes, but the initial condition used in the simulations is not easily realized in physical experiments. However, concentrations of additives or active components at different spatial locations are measured routinely. Thus, we next consider the dispersion of a dye blob as a function of the Reynolds number in the following section. The dye is represented initially by a blob of 400,000 fluid tracer particles, distributed uniformly along the surface of a sphere (its diameter equal to 3 mm). Such an initial condition could be closely approximated in the laboratory using a pipette. The large number of tracer particles used in this method is needed in order to resolve the spatial variation of tracer concentration with sufficient detail. It should be stressed that the initial conditions in the simulation and the experiment need not match too closely because mixing patterns asymptotically overlay the global unstable manifold of the flow, creating mixing structures that are independent of time and initial conditions (Muzzio et al., 2000). The center of the blob in each case was aligned with one of the impeller blades and was 0.0946 m away from the shaft and 0.1825 m from the bottom of the tank. With this initial condition, the entire blob is in the upper half of the vessel. It is expected that significant vertical heterogeneity in dye concentration will be observed, because the flow is strongly compartmentalized.

We considered the percentage of the flow volume that is invaded by the dye as a measure of mixing performance at different impeller speeds. Particle positions were recorded after every 10 revolutions up to a total of 400 impeller rotations. We focus on radial and vertical heterogeneity of tracer concentrations. Azimuthal variations were neglected in the

data analysis, because a statistically meaningful resolution of particle concentrations in three dimensions would make the computations prohibitive. Given the largely axisymmetric geometry of the system, significant variations in concentration along the angular direction disappear rapidly in a matter of a few impeller revolutions.

We computed the amount of tracer in each region of the tank by dividing the volume into annular cells with 51 radial and 153 vertical divisions, that is, each cell is a ring with a square cross-section. Then, the concentration of particles in each volume cell is simply equal to the number of particles that fall within a cell divided by the volume of the cell. The percentage of the flow domain V_i, that is invaded by tracer particles, is a measure of homogeneity at a given time during the mixing process. In other words, V_i is simply the sum of the volumes of all tori that contain tracer particles divided by the total fluid volume.

Figure 8 shows V_i as a function of the number of impeller revolutions for $Re = 20$, 40, 80, and 160. Substantial differences in the evolution and behavior of these systems can be noted for these four flow conditions. The initial slope of the curves increases with increasing Reynolds numbers indicating a higher rate of volume invasion in the early part of the process. For instance, consider the state of the system after 150 impeller revolutions. The tracer injected in the $Re = 20$ flow is distributed throughout only 20.9% of the total volume. As the impeller speed is increased, the blob covers an increasingly larger fraction of the total fluid volume: V_i is equal to 51.4% at $Re = 40$, 59.2% at $Re = 80$, and 67.9% at $Re = 160$, respectively. However, this trend does not hold true for later times in the mixing process. The rate of tracer distribution remains the slowest in the $Re = 20$ case, where V_i reaches 65.4% by the end of 400 impeller revolutions. The maximum amount of volume coverage is produced by the $Re = 40$ flow

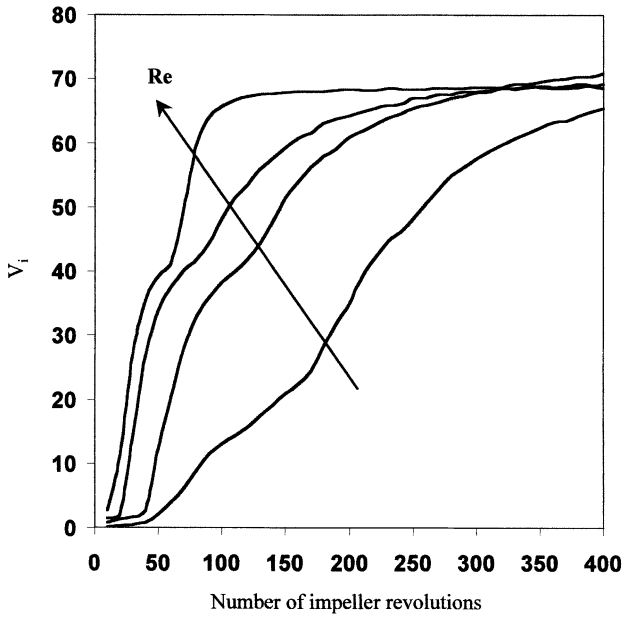

Figure 8. Percentage of the total volume invaded by tracer particles vs. number of impeller revolutions for $Re = 20$, 40, 80, and 160.

(V_i is 70.9%), and is lower for the two highest Re cases after the same number of revolutions: 69.2% for $Re = 80$, and 68.6% for $Re = 160$, respectively. These observations confirm that predicting the evolution and final state of a laminar mixing process is not a trivial task. An important message in the observed trends is that the highest allowable agitation rate in the laminar regime is not necessarily the most effective strat-

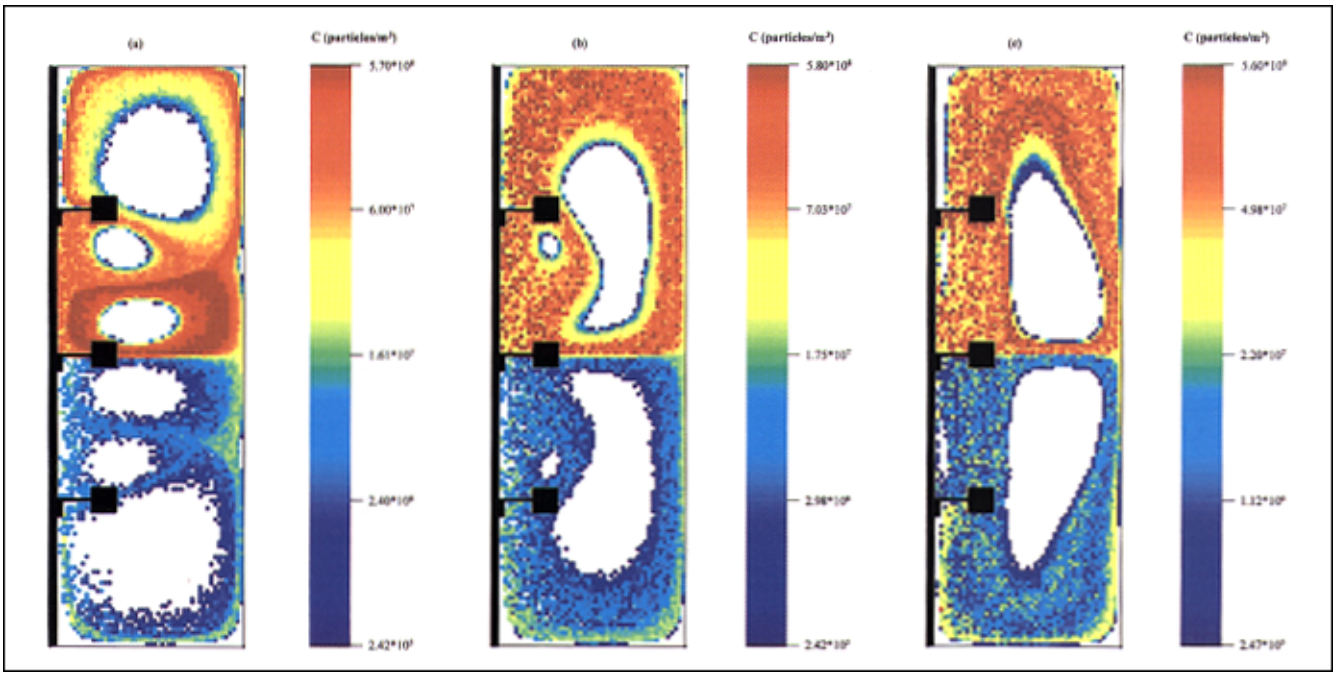

Figure 9. Contour plots of tracer concentrations for $Re = 20$, 40, and 160, in (a)-(c). Segregated regions in the tank remain devoid of tracer particles even after 400 impeller revolutions.

egy. Clearly, the combination of experimental and computational tools presented here could be used to perform a detailed optimization of mixing performance based on time, energy consumption, and so on. Such an analysis is beyond the scope of this article and is left for future communications.

The spatial distribution of the dye in each flow is given by Figure 9 at the end of 400 impeller revolutions. As before, a representative vertical cross-section, aligned with one of the six impeller blades, is chosen in the tank. The images in Figures 9a–9c correspond to $Re = 20$, 40, and 160, respectively (some animations can be seen at http://sol.rutgers.edu/~zalcjm/conc.html). In each case, the color-coding of the cells is based on the concentration of tracer particles in each ring (that is, the results represent the average concentration along the azimuthal direction). The lowest values of C are plotted in dark blue, followed by light blue, green, yellow, orange, and red in ascending order. Areas not invaded by the tracer are colored white.

The immediate observation at all flow conditions is the strong segregation along the vertical direction, which was also forecasted by the stretching fields in Figures 4a–c. The results reveal a great deal of spatial heterogeneity in tracer concentration, despite injecting the dye blob initially in the chaotic region of the flow. Exchange of material between the upper and the lower half of the vessel is minimal due to flow compartmentalization and poor vertical mixing. A plane of separation at the mid-height of the tank is clearly visible even after 400 impeller revolutions for all flows.

It is interesting to compare the mixing intensity predicted by the stretching field for $Re = 20$ (Figure 4a) and the tracer concentration field (Figure 9a). The six regular flow regions, indicated by very low stretching values in Figure 4a, remain completely devoid of tracer after 400 impeller revolutions. The fastest rate of tracer distribution in Figure 9a corresponds closely to the high-stretching regions in Figure 4a. Figure 9b shows the tracer concentration field for $Re = 40$ at the end of 400 impeller revolutions. Again, the regions lacking tracer particles reveal the large kidney-shaped islands seen earlier in Figure 4b. The pair of small islands between the impellers also corresponds closely to empty regions in Figure 9b. These small segregated regions disappear for the two highest *Re* flows, but the large islands remain and shift closer to the vessel wall. The concentration field for the highest flow rate case, $Re = 160$, is indicated in Figure 9c.

A detailed study of the evolution of tracer concentration fields as a function of the Reynolds number, which is clearly possible both by the computational tools discussed here and by quantitative experimental techniques, will be communicated in future publications.

Conclusions

Laminar mixing performance in a stirred tank equipped with three Rushton turbines was studied computationally for a range of Reynolds numbers ranging from 20 to 200. It was confirmed that laminar flows in this range are partially chaotic and possess large, poor-mixing segregated regions whose size and shape depends strongly on the agitation rate. Micromixing intensities were computed based on the stretching field to illustrate permanent spatial variations in mixing rates and to quantify the level of chaotic behavior present for each condition. The dynamics of partially mixed structures was investigated by particle tracking methods and compared with experimental visualizations of the mixing structure at various *Re* numbers. Excellent agreement was attained between simulated mixing structures and experimental ones obtained by planar laser-induced fluorescence.

The computational results further elucidate the mechanism of laminar mixing in stirred tanks: the impeller blades cause reorientation of fluid elements. The resulting mixing structures become elongated as they are deflected by the impeller blades and result in an iterative chaotic mixing process that is phenomenologically identical to processes studied in the past two decades in 2-D model systems. This knowledge can be exploited in future work to develop techniques for optimally designing mixing processes.

An interesting observation, contrary to intuition, is that higher *Re* does not necessarily lead to more efficient mixing. The size and location of unmixed regions also depends on *Re* in a nonintuitive manner. Furthermore, optimal injection locations, mixing rates, and concentration profiles all show nontrivial dependence on *Re*. Clearly, since the parameter space is simply too large to explore experimentally, the practitioner needs access to CFD toolboxes in order to undertake optimal design of laminar mixing processes.

Literature Cited

Alvarez, M. M., F. J. Muzzio, S. Cerbelli, A. Adrover, and M. Giona, "Self-Similar Spatiotemporal Structure of Intermaterial Boundaries in Chaotic Flows," *Phys. Rev. Lett.*, **81**, 3395 (1998).

Alvarez, M. M., T. Shinbrot, J. M. Zalc, and F. J. Muzzio, "The Mechanisms of Chaotic Mixing in Stirred Tanks," *Chem. Eng. Sci.*, in press (2002).

Aref, H., "Stirring by Chaotic Advection," *J. Fluid Mech.*, **143**, 1 (1984).

Bakker, A., and R. LaRoche, "Flow and Mixing with Kenics Static Mixers." *Cray Channels*, **15**, 25 (1993).

Bakker, A., K. J. Myers, R. W. Ward, and C. K. Lee, "The Laminar and Turbulent Flow Pattern of a Pitched Blade Turbine," *Trans. IChemE*, **74A**, 485 (1996).

Biggs, R. D., "Mixing Rates in Stirred Tanks," *AIChE J.*, **9**, 636 (1963).

Cherry, R. S., and E. T. Papoutsakis, "Physical Mechanisms of Cell Damage in Microcarrier Cell Culture Bioreactors," *Biotech. Bioeng.*, **32**, 1001 (1988).

Derksen, J., and H. E. Van den Akker, "Large Eddy Simulations on the Flow Driven by a Rushton Turbine," *AIChE J.*, **45**, 209 (1999).

Distelhoff, M. F., A. J. Marquis, J. M. Nouri, and J. H. Whitelaw, "Scalar Mixing Measurements in Batch Operated Stirred Tanks," *Can. J. Chem. Eng.*, **75**, 641 (1997).

Godfrey, J. C., "Mixing of Liquids in Stirred Tanks," *Mixing in the Process Industries*, N. Harnby, M. F. Edwards, and A. W. Nienow, eds., Butterworth, New York (1992).

Harvey III, A. D., and S. E. Rogers, "Steady and Unsteady Computation of Impeller-Stirred Reactors," *AIChE J.*, **42**, 2701 (1996).

Harvey III, A. D., D. H. West, and N. B. Tufillaro, "Evolution of Laminar Mixing in Stirred Tanks using a Discrete-Time Particle-Mapping Procedure," *Chem. Eng. Sci.*, **55**, 667 (2000).

Hayes, R. E., A. Afacan, B. Boulanger, and P. A. Tanguy, "Experimental Study of Reactive Mixing in a Laminar Flow Batch Reactor," *Trans. IChemE*, **76**, 73 (1998).

Hobbs, D. M., and F. J. Muzzio, "The Kenics Static Mixer: a Three-Dimensional Chaotic Flow," *Chem. Eng. J.*, **67**, 153 (1997).

Holden, P. J., M. Wang, R. Mann, F. J. Dickin, and R. B. Edwards, "Imaging Stirred-Vessel Macromixing using Electrical Resistance Tomography," *AIChE J.*, **44**, 780 (1998).

Kramers, H., G. M. Baars, and W. H. Knoll, "A Comparative Study on the Rate of Mixing in Stirred Tanks," *Chem. Eng. Sci.*, **2**, 35 (1953).

Kresta, S. M., and P. E. Wood, "Prediction of the Three-Dimensional Turbulent Flow in Stirred Tanks," *AIChE J.*, **37**, 448 (1991).
Lamberto, D. J., M. M. Alvarez, and F. J. Muzzio, "Experimental and Computational Investigation of the Laminar Flow Structure in a Stirred Tank," *Chem. Eng. Sci.*, **54**, 919 (1999).
Muzzio, F. J., P. D. Swanson, and J. M. Ottino, "The Statistics of Stretching and Stirring in Chaotic Flows," *Phys. Fluids A*, **3**, 822 (1991).
Muzzio, F. J., P. D. Swanson, and J. M. Ottino, "Mixing Distributions Produced by Multiplicative Stretching in Chaotic Flows," *Int. J. Bifurc. Chaos*, **2**, 1 (1992).
Muzzio, F. J., M. M. Alvarez, S. Cerbelli, M. Giona, and A. Adrover, "The Intermaterial Area Density Generated by Time- and Spatially Periodic 2D Chaotic Flow," *Chem. Eng. Sci.*, **55**, 1497 (2000).
Naude, I. N., C. Xuereb, and J. Bertrand, "Direct Prediction of the Flows Induced by a Propeller in an Agitated Vessel Using an Unstructured Mesh," *Can. J. Chem. Eng.*, **76**, 631 (1998).
Norwood, K. W., and A. B. Metzner, "Flow Patterns and Mixing Rates in Agitated Vessels," *AIChE J.*, **6**, 432 (1960).
Ranade, V. V., "An Efficient Computational Model for Simulating Flow in Stirred Vessels: a Case of Rushton Turbine," *Chem. Eng. Sci.*, **52**, 4473 (1997).
Rauline, D., P. A. Tanguy, J. LeBlévec, and J. Bousquet, "Numerical Investigation of the Performance of Several Static Mixers," *Can. J. Chem. Eng.*, **76**, 527 (1998).
Sahu, A. K., P. Kumar, A. W. Patwardhan, and J. B. Joshi, "CFD Modeling and Mixing in Stirred Tanks," *Chem. Eng. Sci.*, **54**, 2285 (1999).
Shane, M. S., J. Hamel, and D. I. Wang, "Hydrodynamic Effects on Animal Cells Grown in Microcarrier Cultures," *Biotech. Bioeng.*, **29**, 130 (1987).
Smith III, F. G., "A Model of Transient Mixing in a Stirred Tank," *Chem. Eng. Sci.*, **52**, 1459 (1997).
Wittmer, S., L. Falk, P. Pitiot, and H. Vivier, "Characterization of Stirred Vessel Hydrodynamics by Three Dimensional Trajectography," *Can. J. Chem. Eng.*, **76**, 600 (1998).
Zalc, J. M., E. S. Szalai, and F. J. Muzzio, "Characterization of Flow and Mixing in the SMX Static Mixer," *AIChE J.*, **48**, 427 (2002).
Zalc, J. M., M. M. Alvarez, and F. J. Muzzio, "Extensive Validation of Computed Laminar Flow Fields in a Stirred Tank Equipped with Three Rushton Turbines," *AIChE J.*, **47**, 2144 (2001).

Manuscript received Oct. 5, 2001, and revision received Feb. 7, 2002.